Multinuclear NMR Investigation of $Al(N0_3)_3$ and Morpholine Dissolved in Water, in the Presence and Absence of HF

E. W. Hansen,*,† Ø. B. Vistad,†,‡ D. E. Akporiaye,† K. P. Lillerud,‡ and R. Wendelbo†

SINTEF Applied Chemistry, P.O. Box 124 Blindern, 0314 Oslo, Norway, and Department of Chemistry, University of Oslo, P.O. Box 1033, Blindern, 0315 Oslo, Norway

Received: July 15, 1998

Multinuclear (^{27}A1, ^{19}F, ^{13}C, and ^{1}H) NMR measurements at room temperature of aqueous solutions containing 2 M $Al(NO_3)_3$, 2.1 M morpholine, in the presence and absence of 1 M HF, suggest that morpholine is a chemically inactive specie. The proton and carbon chemical shifts of morpholine in the two solutions reveal the same pH dependence, suggesting that morpholine can be used as a probe molecule for pH determination. Moreover, the broad peaks observed in the ^{19}F and ^{27}A1 NMR spectra are consistent with the formation of multinuclear Al species and Al−F complexes. The observed changes in peak intensities of these same nuclei as a function of pH are in semiquantitative agreement with corresponding intensities calculated from chemical equilibrium reaction models. A more detailed spectral analysis reveals some discrepancies between observed and calculated intensities and is discussed in the text.

Introduction

SAPO's are crystalline microporous materials with pores of molecular dimensions.[1,2] The synthesis of such molecular sieves requires a source of water, silicon, aluminium, and phosphorous, and an organic structure directing agent (usually an amine). For instance, pure trigonal SAPO-34 crystals are obtained after 48 h at 200 °C from a solution having the following reactant composition (mole ratio): 1.0 SiO_2, 1.0 $A1_2O_3$, 1.0 P_2O_5, 2.1 morpholine, 60 H_2O.[3] Recently, it has been shown that when mixing 1 equiv of HF into the former gel solution, a mixture of triclinic and trigonal SAPO-34 crystals are formed,[4] which after calcination at 580 °C in air gives pure trigonal SAPO-34 crystals.

Generally, the synthesis of molecular sieves involves three interacting phases: a solution phase, an amorphous gel, and a crystalline solid.[5] The relative distribution of these phases will depend on the concentration of reactants as well as on the pH of the solution. The latter is expected to change significantly during the initial stage of the synthesis reaction.[6]

A first NMR experimental trial to identify the numerous species (complexes) formed in a synthesis solution was found to be surprisingly demanding. In particular, rather broad, featureless bands were observed in the ^{27}Al NMR spectra due to severe overlap of peaks. In spite of the better spectral resolution observed in the ^{19}F, ^{31}P, ^{1}H, and ^{13}C NMR spectra of such a synthesis solution (at room temperature), a detailed picture of the different chemical species and their relative concentration was difficult to ascertain.[7]

To resolve some of these complexities, we found it advantageous to investigate less complex solutions (containing less number of reactants) under the constraint that the applied reactant concentrations are the same as in the synthesis solution. This approach has been adopted by many authors during the last 2 or 3 decades.[8−28] However, most of these investigations have been restricted to solutions of low ionic strength or within pH ranges where no solids or gels are being formed. To our knowledge, the most recent and detailed work involving this simplified strategy has been reported by Mortlock et al.,[5,24] who characterized aqueous solutions of orthophosphoric acid, aluminium chloride, and tetramethylammonium (TMA) hydroxide in order to gain more insight into the synthesis of crystalline AIPO4 materials.

The requirement of an organic structure directing agent for the occurrence of crystallisation of SAPO's prompted us to use NMR spectroscopy to characterize solutions containing only one reagent species together with morpholine under different acidity (pH) conditions. The main object is to chart the spectral details and complexities observed in the NMR spectra of real SAPO synthesis solutions.[7] The observation that HF plays an important role in the synthesis of SAPO's[4] made it attractive to also include HF as a reactant species in the present NMR investigation. Thus, a detailed, multinuclear NMR analysis of two different aqueous solutions containing $Al(NO_3)_3$ and morpholine with and without the addition of HF will be reported. The analysis will cover the pH range from 0.5 to 13.5 in which solids, gels, and a solution phase may coexist.

The choice of reactant concentrations used in this work was dictated by literature reports on the optimal synthesis conditions used to form SAPO crystals;[3,4] i.e., a mole ratio of $Al(NO_3)_3$: morpholine:HF = 2:2.1:1, respectively.

Experimental Section

Materials. Two aqueous "reference" solutions containing 2 M $Al(NO_3)_3$ and 2.1 M morpholine (solution A) and 2 M $Al(NO_3)_3$, 2.1 M morpholine, and 1 M HF (solution B), respectively, were prepared. These solutions were diluted with either 6 M HNO_3 or 6 M NaOH to obtain the desired pH. The resulting test solutions and their corresponding pHs are summarized in Table 1. The pH was determined by a pH indicator with an inherent uncertainty of approximately ±0.5 pH units. Also, the density of the solutions were determined, enabling the molar

* To whom correspondence should be addressed.
† SINTEF Applied Chemistry.
‡ University of Oslo.

10.1021/jp983023x CCC: $18.00
Published on Web 03/13/1999

TABLE 1: Composition and pH of Test Samples Prepared by Dilution of Reference Sample with 6 M HNO_3 or 6 M NaOH

weight of sample (g)	weight of acid/base (g)	pH	solution characteristics
A. Sample A (2 M $Al(NO_3)_3$ and 2.1 M Morpholine)			
7.50	7.50 (HNO_3)	0.5	clear
7.52	2.02 (HNO_3)	1	clear
7.49	1.00 (HNO_3)	2	clear
7.50		3	clear
7.50	1.10 (NaOH)	4	clear
7.50	3.00 (NaOH)	6.5	turbid
7.51	3.50 (NaOH)	8	turbid
7.51	5.10 (NaOH)	10	turbid
7.51	6.00 (NaOH)	12.5	clear
B. Sample B (2 m $Al(NO_3)_3$, 2.1 M Morpholine, and 1 M HF)			
7.53	5.00 (HNO_3)	0.5	clear
7.50	*x* (HNO_3)	1	clear
7.50	0.80 (HNO_3)	1.5	clear
7.50		2.5	clear
7.53	1.50 (NaOH)	4	clear
7.50	2.75 (NaOH)	4.5	turbid
7.51	3.50 (NaOH)	7	turbid
7.51	5.00 (NaOH)	10	turbid
7.51	6.00 (NaOH)	11	turbid
7.50	9.30 (NaOH)	13.5	clear

concentration to be calculated and the expected NMR signal intensity of each species to be estimated.

NMR. The NMR measurements were performed at room temperature (25 °C) on a Varian VXR spectrometer operating at 300 MHz proton resonance frequency. The solution was confined in a 5 mm o.d. tube which was inserted into an NMR tube of diameter 10 mm. The resulting free space between the two tubes was filled with D_2O, which was used as a lock solvent.

To acquire quantitative NMR spectra, the repetition time was chosen to be about 5 times the longest spin−lattice relaxation time (T_1) for each of the nuclei investigated (^1H, ^{19}F, ^{13}C, and ^{27}Al). Regarding the ^{27}Al NMR experiments, a shortest possible pulse angle (corresponding to a rf pulse of 0.5 μs) was used in order to minimize the effect of signal decay during the pulse. This precaution was found necessary due to short spin−spin relaxation times combined with a potentially large quadrupolar coupling constant. Signal intensity (area) was determined by numerical integration of the resonance peak or by mathematical deconvolution when severe overlap of peaks was observed.

Of particular importance, both ^{19}F and ^{27}Al NMR revealed broad background signals originating from the probe design. To avoid interference from this unwanted signal in the quantitative analysis, the first few points in the NMR free induction decay (FID) were deleted and a linear (back) prediction algorithm was applied.[29] This approach was possible since all resonance peaks revealed Lorenzian line shape profiles.[30]

All chemical shift measurements have been referenced to external liquid solutions, i.e., TMS (^1H and ^{13}C), $Al(NO_3)_3$ (^{27}Al), and CFCl3 (^{19}F).

Results and Discussion

^1H NMR. Both the line width and chemical shift of the solvent water peak of solution B (Figure 1) reveal significant changes as a function of pH. A similar behavior is observed for solution A (spectra not shown) and suggests that addition of HF does not affect the appearance of the water resonance peak in the spectrum when the spectrum is acquired at the same pH. The sudden drop in chemical shift (Figure 2) and the corresponding increase in line width (Figure 1) at pH = 1 are not fully understood but may originate from a change in the exchange rate of water molecules between bulk water and the $Al(H_2O)_6^{3+}$ complex at this pH according to the reaction

$$Al(H^*_2O)_6^{3+} + HOH \leftrightarrow Al(H_2O)_6^{3+} + HOH^*$$

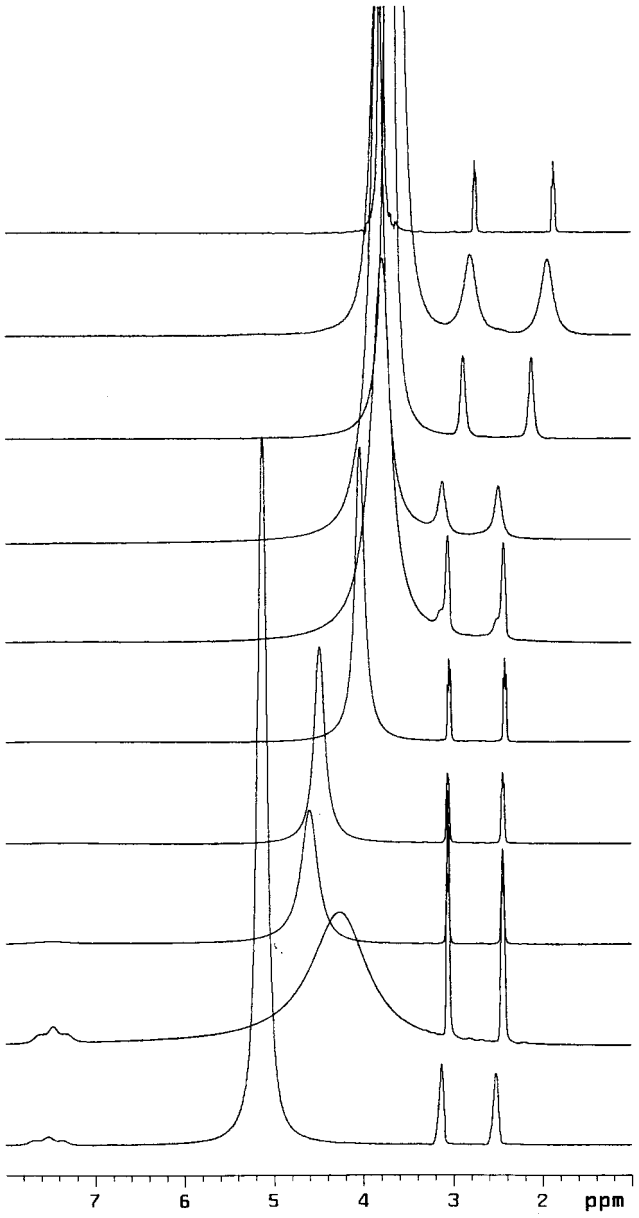

Figure 1. ^1H NMR spectra of solution B (2 M $Al(NO_3)$, 2.1 M morpholine, and 1 M HF in water) vs pH (=0.5, 1, 1.5, 2.5, 4, 4.5, 7, 10, 11, and 13.5 from bottom to top).

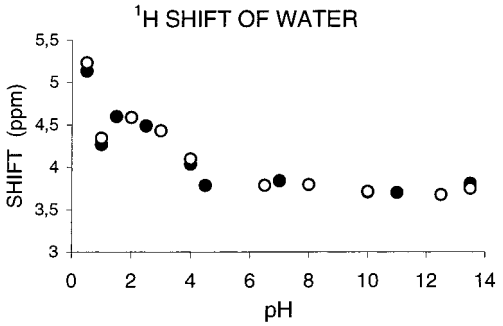

Figure 2. ^1H NMR chemical shift of the water peak vs pH of solutions A ((○) 2 M $Al(NO_3)_3$, 2.1 M morpholine in water) and B ((●) 2 M $Al(NO_3)_3$, 2.1 M morpholine, and 1 M HF in water).

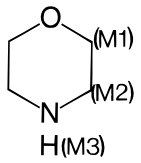

Figure 3. Structure of morpholine.

Except for this dramatic decrease in chemical shift at approximately pH = 1, the chemical shift shows an overall decrease with increasing pH up to pH = 4, above which the chemical shift is approximately constant. Note also the appearance of a broad triplet band at low pH with a chemical shift δ = 7.5 ppm (M3; Figure 3) which is assigned to the −NH proton of morpholine.

The triplet is caused by a coupling of the proton to the quadrupolar nucleus, ^{14}N with spin = 1. The reason that the triplet does not split into three equally intense lines in the spectrum originates from a combined effect of a rapid spin−lattice relaxation time (T_1) of the ^{14}N nucleus and the size of the scalar coupling constant (J_{NH}) between the proton and the quadrupolar neucleus.[30] However, for most NH groups the situation is more complex due to the existence of real proton exchange between the NH proton and the water protons, i.e.,

$$NH^* + H_2O \leftrightarrow NH + HOH^*$$

Depending on the exchange rate of this reaction, the line shape (and chemical shift) of both the water resonance and the amine proton resonance will be affected. Thus, the disappearance of the triplet peak in the spectrum with increasing pH, the sudden decrease in chemical shift, and the marked increase in line width of the water peak at low pH may originate from changes in the exchange rate as a function of pH.[30] It is worth noting that, if the exchange rate is fast on the NMR time scale, the amine proton resonance and the water resonance will coalesce and only a single line will appear in the spectrum.

The two proton resonance peaks observed at the higher magnetic field (Figure 1) represent the two nonequivalent $-CH_2-$ groups of morpholine (M1 and M2; Figure 3) and reveal some fine structure at low pH (intramolecular coupling). This fine structure is absent at pH > 4, where the lines become much broader. It is interesting to note that this line broadening becomes significant only when the solution becomes more turbid. This is probably due to a susceptibilty effect, caused by precipitation of small particles into the solution. With increasing pH (pH ≥ 13.5), the solution becomes again clear and the same fine structure as seen at low pH reappears in the spectrum.

The chemical shift of the two nonequivalent groups of methylene protons of morpholine is shown in Figure 4 and is approximately independent of pH up to about pH = 8. Above this pH, the chemical shift decreases and reaches a constant value for pH > 12. If comparing the chemical shift of these peaks within solutions A (no HF) and B (addition of HF), no difference can be observed as a function of pH, and this is rationalized as follows.

Morpholine can exist in both an acid form (XH_2^+) and a base form (XH) depending on the pH of the solution (eq 1).

$$XH_2^+ \leftrightarrow XH + H^+ \qquad (1)$$

Denoting the chemical shift of the acid form by $\delta_0(XH_2^+)$ and the corresponding chemical shift of the base form by $\delta_0(XH)$, the observable chemical shift (δ), under fast exchange conditions, can be written

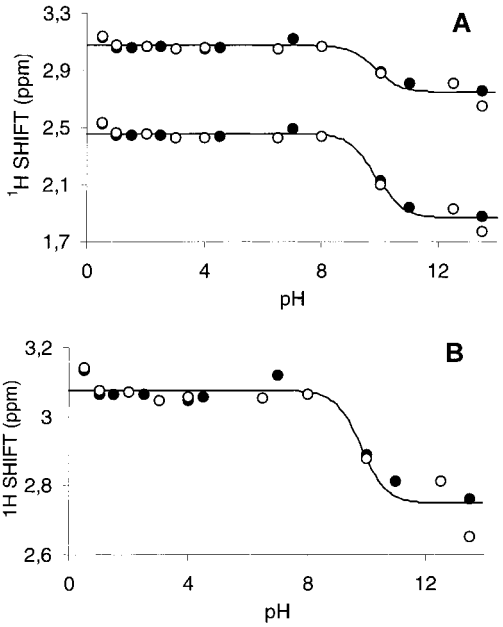

Figure 4. (A) ^{1}H NMR chemical shift of the two methylene protons M1 and M2 of morpholinre (Figure 3) vs pH of solutions A ((○) 2 M $Al(NO_3)$, 2.1 M morpholine in water) and B ((●) 2 M $Al(NO_3)$, 2.1 M morpholine, and 1 M HF in water). (B) Expanded view of part A. The solid curves in both parts represent model calculations and are described in the text.

$$\delta = f(XH_2^+)\delta_0(XH_2^+) + f(XH)\delta_0(XH) \qquad (2a)$$

where f(X) defines the mole fraction of species X (XH_2^+ or XH),

$$f(X) = \frac{[X]}{[XH_2^+] + [XH]} \qquad (2b)$$

and [ ] represents the molar concentration. Denoting the acid/base equilibrium constant of morfoline by K_a,

$$K_a = \frac{[H^+][XH]}{[XH_2^+]} \qquad (2c)$$

Equations 2a−c can be combined to give the chemical shift (δ) as a function of K_a and pH:

$$\delta = \frac{\delta_0(XH_2^+) + K_a 10^{pH}\delta_0(XH)}{1 + K_a 10^{pH}} \qquad (3)$$

Since the $-NH_2$ proton peak broadens and disappears at a relatively low pH, eq 3 can not be used to analyze this particular chemical shift as a function of pH. However, since the change in chemical shift is caused by a change in the electronic environment, it is expected that the electronic environment of the methylene protons will be affected accordingly (inductive effect). The chemical shift of these methylene protons as a function of pH is shown in Figure 4 where the solid curves represent nonlinear least-squares fits to eq 3. The numerical results are summarized in Table 2 and show that the derived K_a values are, within experimental uncertainty, identical. However, they deviate somewhat from earlier published values of pK_a (=8.33).[31]

TABLE 2: K_a Values and Chemical Shifts (Proton and Carbon) of the Acid Form and the Base Form of the Methylene Groups in Morpholine as Derived by Fitting Eq 3 to the Observed Chemical Shifts vs pH (Figures 3 and 5) of Solutions A (2 M $Al(NO_3)_3$ and 2.1 M morpholin) and B (2 M $Al(NO_3)_3$, 2.1 M morpholine, and 1 M HF)[a]

peak assignment	pK_a	δ (acid form) (ppm)	δ (base form) (ppm)
Ml (proton)	9.82	3.076	2.748
M2 (proton)	9.80	2.459	1.867
M1 (carbon)	9.80	72.439	75.849
M2 (carbon)	9.86	52.225	53.435

[a] For peak assignment, see Figure 1.

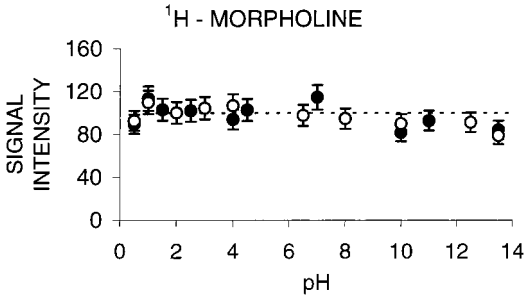

Figure 5. ^1H NMR signal intensity of the methylene proton peak (M 1) in morpholine vs pH of solutions A ((○) 2 M $Al(NO_3)_3$, 2.1 M morpholine in water) and B ((●) 2 M $Al(NO_3)_3$, 2.1 M morpholine, and 1 M HF in water). The dotted line represents the signal intensity if all morpholine is detectable by NMR.

It may be possible that in the intermediate pH range, where solid particles are formed, morpholine may coprecipitate from the solution. Precipitated morpholine (solid) will not be detectable by high-resolution NMR, except if there is a fast exchange of morpholine between the solid phase and the liquid phase. Figure 5 suggests that the observed proton signal intensity of morpholine is, within experimental uncertainty, constant and independent of pH (dotted line in Figure 5). Thus, NMR presents no experimental evidence for any precipitation of morpholine.

^{13}C NMR. As discussed in the previous section, the fraction of the acid/base forms of morpholine as a function of pH strongly affects the observed proton chemical shift of the methylene groups in morpholine. A corresponding change in chemical shift of the methylene carbons is thus expected and is confirmed by the experimental results presented in Figure 6. Fitting eq 3 to these data enables the extraction of pK_a, which is found to be identical to pK_a derived from proton NMR measurements (Table 2). Moreover, the chemical shifts of the methylene carbons of the acid and base forms in morpholine are determined. The numerical results are summarized in Table 2. These results confirm the internal consistency between carbon and proton NMR chemical shifts of morpholine.

Figure 6B shows an expanded view of one of the methylene carbon (M1) chemical shifts as a function of pH and reveals a significant but small decrease in chemical shift as a function of pH in the range pH = 0.5−5. This observation may originate from the pH dependence of the exchange rate of the amine protons with the water protons, as discussed in the previous section. A similar observation can not be inferred from the proton chemical shift measurements. Anyhow, this result suggests that the template molecule can be used as a probe molecule for pH in the range 8−10. It is expected, however, that if morpholine interacts with other reagents in the solution, the chemical shift will change accordingly. This may, in turn, give rise to chemical shifts outside the chemical shift region presented in Figures 4 and 6. To monitor the chemical shift of morpholine as a function of reaction time under real SAPO synthesis conditions may therefore give valuable insight as to the fate of this structure-directing molecule.

^{27}Al NMR. Figure 7 presents ^{27}Al NMR spectra of solution B as a function of pH and shows no observable signal intensity in the pH range from approximately 4.5 to 11. This same trend in spectral appearance is also observed for solution A (not shown) with a slight difference; within the pH range of approximately 3−4 (Figure 8), the observed signal intensity of solution B is somewhat more intense compared to the signal intensity of solution A.

To rationalize these findings, the following two sets of reaction schemes were applied:[32]

$$Al^{3+} + H_2O \rightleftharpoons Al(OH)^{2+} + H^+ \qquad K_{11} = 10^{-4.97} \quad (4a)$$

$$Al^{3+} + H_2O \rightleftharpoons Al(OH)^{2+} + 2H^+ \qquad K_{12} = 10^{-9.3} \quad (4b)$$

$$Al^{3+} + 3H_2O \rightleftharpoons Al(OH)_3(s) + 3H^+ \qquad K_{13} = 10^{-8.5} \quad (4c)$$

$$Al^{3+} + 4H_2O \rightleftharpoons Al(OH)_4^- + 4H^+ \qquad K_{14} = 10^{-23} \quad (4d)$$

$$2Al^{3+} + 2H_2O \rightleftharpoons Al_2(OH)_2^{4+} + 2H^+ \qquad K_{15} = 10^{-7.7} \quad (4e)$$

$$3Al^{3+} + 4H_2O \rightleftharpoons Al_3(OH)_4^{5+} + 4H^+ \qquad K_{16} = 10^{-13.9} \quad (4f)$$

$$13Al^{3+} + 4H_2O \rightleftharpoons Al_{13}O_4(OH)_{24}^{7+} + 32H^+ \qquad K_{17} = 10^{-98.7} \quad (4g)$$

and[33]

$$AlF^{2+} \rightleftharpoons Al^{3+} + F^- \qquad K_{21} = 10^{-7.01} \quad (5a)$$

$$AlF_2^+ \rightleftharpoons Al^{3+} + 2F^- \qquad K_{22} = 10^{-12.75} \quad (5b)$$

$$AlF_3 \rightleftharpoons Al^{3+} + 3F^- \qquad K_{23} = 10^{-17.02} \quad (5c)$$

$$AlF_4^- \rightleftharpoons Al^{3+} + 4F^- \qquad K_{24} = 10^{19,72} \quad (5d)$$

$$AlF_5^{2-} \rightleftharpoons Al^{3+} + 5F^- \qquad K_{25} = 10^{20.91} \quad (5e)$$

$$AlF_6^{3-} \rightleftharpoons Al^{3+} + 6F^- \qquad K_{26} = 10^{20.86} \quad (5f)$$

$$HF \rightleftharpoons H^+ + F^- \qquad K_{27} = 10^{-3.21} \quad (5g)$$

$$HF_2^- \rightleftharpoons HF + F^- \qquad K_{27} = 10^{-0.59} \quad (5h)$$

The two latter equilibrium constants (eqs 5g and 5h) have been determined in this work and will be discussed in a later section. In addition, the dissociation of water ($H_2O = H^+ + OH^-$) is included in the above reaction scheme. It must be emphasized that the K_{ij} values presented in eqs 5a−f involve molal activities, [i] of species i. For simplicity, we have assumed the activity coefficients of all species to be equal to 1, which is strictly valid only for dilute solutions. Thus, the present discussion will be of a somewhat qualitative nature.

The tridecameric cation,[6] $[AlO_4Al_{12}(OH)_{24}(H_2O)_{12}]^{7+}$ (eq 4g), represents the Al_{13} modified-Keggin structure which has been the subject of much interest for its ability to intercalate clay minerals and produce catalytically active pillard clays. Akitt et al.[6] have assigned this structure to a single, sharp resonance peak in the ^{27}Al NMR spectrum with a chemical shift $\delta = 62.5$

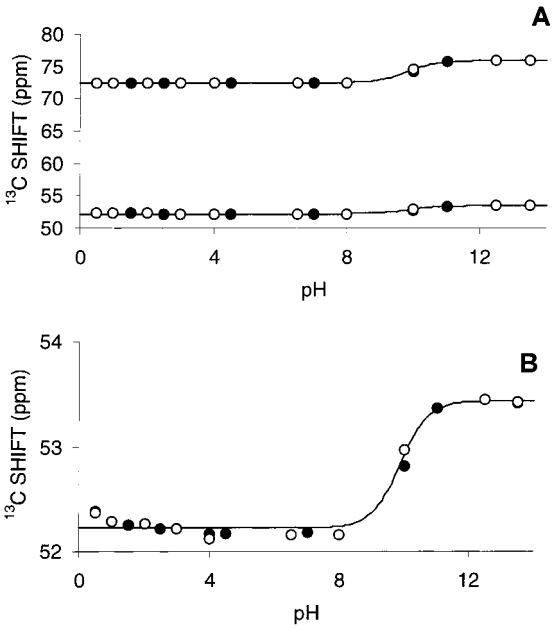

Figure 6. (A) ^{13}C NMR chemical shift of the two methylene carbons, M1 and M2, in morpholine (Figure 3) vs pH of solutions A ((○) 2 M $Al(NO_3)$, 2.1 M morpholine in water) and B ((●) 2 M $Al(NO_3)$, 2.1 M morpholine, and 1 M HF in water). (B) Expanded view of part A). The solid curves represent model calculations as described in the text.

ppm. This peak corresponds to the single tetrahedral aluminum in the "Keggin" structure, since the other 12 ^{27}A nuclei are confined in octahedral positions giving rise to very broad, unobservable resonance peaks. These latter peaks are, however, claimed to be detectable at elevated temperature.[6] In this work, we have not been able to detect a resonance peak at $\delta = 62.5$ ppm. Thus, any formation of this species has been treated as nonobservable. Nor is the solid precipitate $Al(OH)_3$ detectable by high-resolution NMR, and it is treated accordingly. The dotted curve in Figure 8 represents the calculated amount of detectable ^{27}Al NMR signal intensity as a function of pH (eqs 4) of solution A and is in acceptable agreement with observation, except for pH = 12.5, at which the calculated intensity is much larger than the observed intensity. The reason for this discrepancy is poorly understood but may be related to the inherent assumption of ideal, dilute solutions.

When calculating the ^{27}Al NMR signal intensity of solution B from eqs 4 and 5, we have assumed the resonance peaks originating from the $AlF_x^{(3-x)}$ complexes ($x \geq 3$) to be very broad and thus unobservable.[23] The result is shown by the solid curve in Figure 8 and is in acceptable agreement with observation. The reaction model calculations confirm the experimental observation that in the narrow pH range of approximately 2.5−4, more aluminum signal intensity is observable in sample B compared to sample A. This, as will be discussed later, can be explained by the formation of AlF^{2+} and AlF_2^+ complexes.

In addition to the narrow $Al(H_2O)_6^{3+}$ peak at 0 ppm, a much broader peak appears in the ^{27}Al NMR spectra of sample B (Figure 7). In order to investigate this aspect further, expanded (vertical scale) views of the ^{27}Al NMR spectra of samples A and B are shown in parts A and B of Figure 9. A broad peak becomes visible at pH = 2 in solution A, in contrast to solution B where a broad peak appears already at the lowest pH value investigated (pH = 0.5). This suggests that the broad peaks observed in the two solutions have different origins, which must be related to the addition of HF. Due to the severe peak overlap (Figure 9), spectral deconvolution or curve fitting (assuming a Lorenzian lineshape function) was required in order to extract

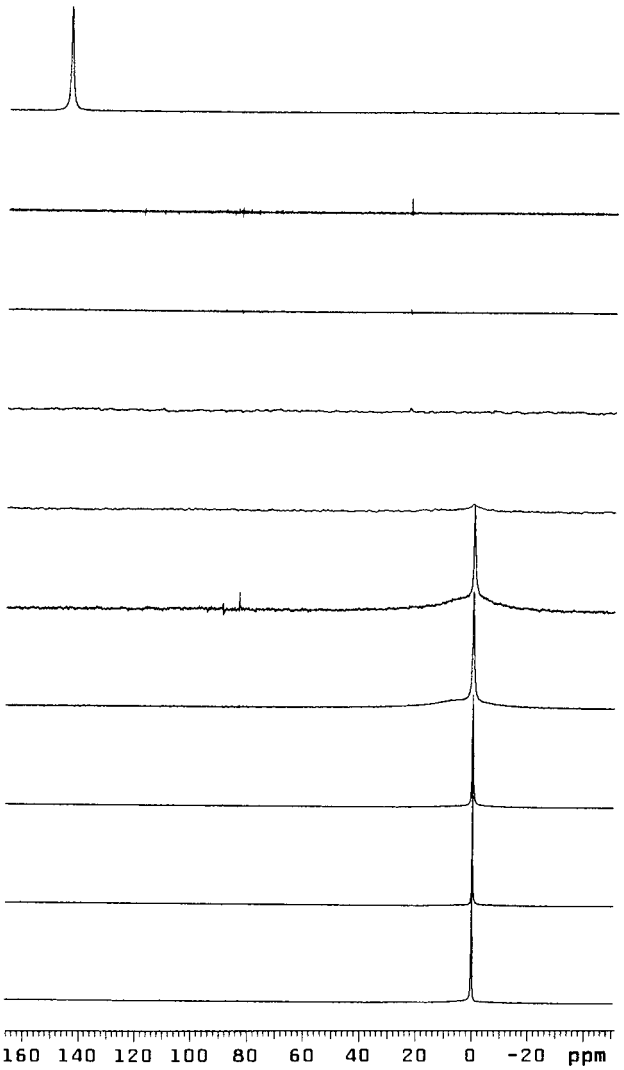

Figure 7. ^{27}Al NMR spectra of solution B (2 M $Al(NO_3)_3$, 2.1 M morpholine, and 1 M HF in water) vs pH (=0.5, 1, 1.5, 2.5, 4, 4.5, 7, 10, 11, and 13.5 from bottom to top).

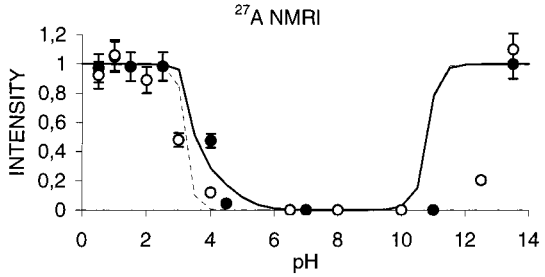

Figure 8. ^{27}Al NMR signal intensity vs pH of solutions A ((○) 2 M $Al(NO_3)_3$, 2.1 M morpholine in water) and B ((●) 2 M $Al(NO_3)_3$, 2.1 M morpholine, and 1 M HF in water). The solid and dotted curves represent calculated signal intensities (eqs 4 and 5), as described in the text.

quantitative information. The results are shown as solid curves in Figure 9. The intensity ratio of the broad and narrow peaks, as well as the linewidth of the broad component, are plotted as a function of pH in Figures 10 and 11, respectively. The broad peak in sample A (observed at pH ≥ 2) is tentatively assigned to the formation 11 of multinuclear Al cations and is supported by previous NMR results reported in the literature.[6] Equations 4e and 4f, which describe the equilibrium formation of dimeric and trimeric Al ions, predict a very small equilibrium concentration of less than 2 mol %. This may imply that the reported

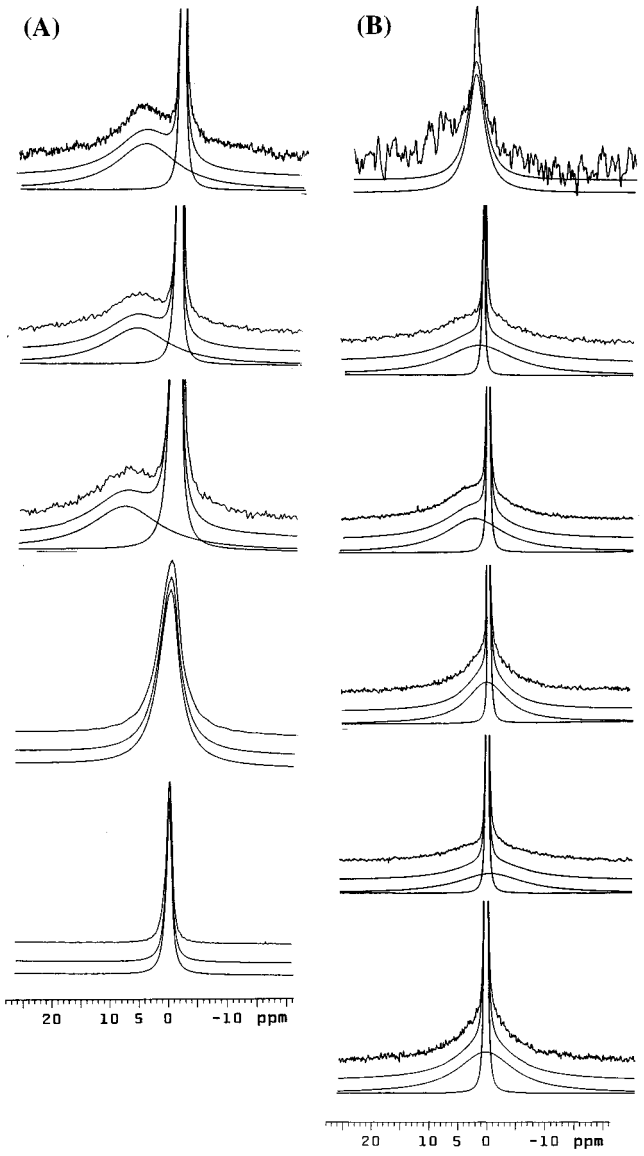

Figure 9. (A) Expanded ^{27}Al NMR spectra of solution A (2 M $Al(NO_3)_3$, 2.1 M morpholine in water) vs pH (=0.5, 1, 2, 3, and 4 from bottom to top). (B) Expanded ^{27}Al NMR spectra of solution B (2 M $Al(NO^3)_3$, 2.1 M morpholine, and 1 M HF in water) vs pH (=0.5, 1, 1.5, 2.5, 4, and 4.5 from bottom to top). Solid curves represent deconvoluted or curve-fitted spectra.

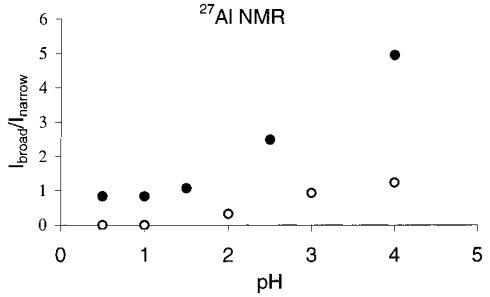

Figure 10. Signal intensity ratio between the broad and the narrow peaks in the ^{27}Al NMR spectra (Figure 9) vs pH of solutions A ((○) 2 M $Al(NO_3)_3$, 2.1 M morpholine in water) and solution B ((●) 2 M $Al(NO_3)_3$, 2.1 M morpholine, and 1 M HF in water).

equilibrium constants of *n*-mers ($n = 2$ and 3) are erroneous or that larger multinuclear species ($n > 3$) may form. This subject needs to be investigated further.

Also, the equilibration of aluminum hydroxide complexes in dilute aqueous solutions is only very slowly achieved and depends both on the OH/Al ratio and how rapidly the solution is initially prepared (mixing time). Lower ratios cause a slower approach to equilibrium. Sometimes equilibrium may not be achieved even after several years of aging. These rather subtle issues are, however, outside the scope of this work.

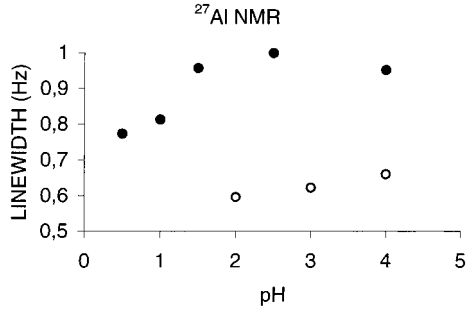

Figure 11. Line width (kHz) of the broad and narrow peak in the ^{27}Al NMR spectra (Figure 8) vs pH of solutions A ((○) 2 M $Al(NO_3)_3$, 2.1 M morpholine in water) and solution B ((●) 2 M $Al(NO_3)_3$, 2.1 M morpholine, and 1 M HF in water).

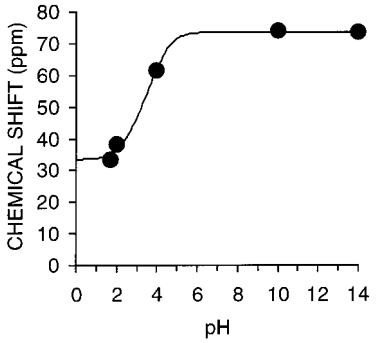

Figure 12. ^{19}F NMR chemical shift of aqueous HF solution (≈1 M) vs pH. Solid curve represents a model fit, as discussed in the text

In solution B, the observed intensity ratio between the broad and the narrow components is approximately 1 at pH = 0.5 and is in quantitative agreement with the formation of AlF^{2+}, according to the reaction $Al^{3+} + F^- \rightarrow AlF^{2+}$, when the initial concentration of $Al(NO_3)_3^{3+}$ and HF are in the ratio 2:1, respectively. This interpretation is also in agreement with the ^{19}F NMR results and will be discussed in the next section. The significantly larger line width of the broad resonance band observed in solution B, compared to the corresponding resonance observed in solution A, may originate from formation of rather different species responsible for these broad resonance bands. This conclusion is supported by the observed difference in intensity (Figure 10) and line width (Figure 11) as a function of pH and will be discussed in the next section.

^{19}F NMR. A few chemical shift measurements of a 1 M HF solution as a function of pH are depicted in Figure 12. The solid curve in Figure 12 is calculated by the same procedure as outlined in a previous section (^{1}H NMR), based on the equilibrium reactions

$$HF \rightleftharpoons H^+ + F^- \quad (6a)$$

$$HF + F^- \rightleftharpoons HF_2^- \quad (6b)$$

This model fit gives $pK_1 = 3.2$ and $pK_2 = 0.59$ where K_1 and K_2 represent the equilibrium constants of reactions 6a and 6b, respectively. However, keeping in mind that the calculated chemical shift is derived (a) under the constraint of a fast exchange process between all F species in solution and (b) the

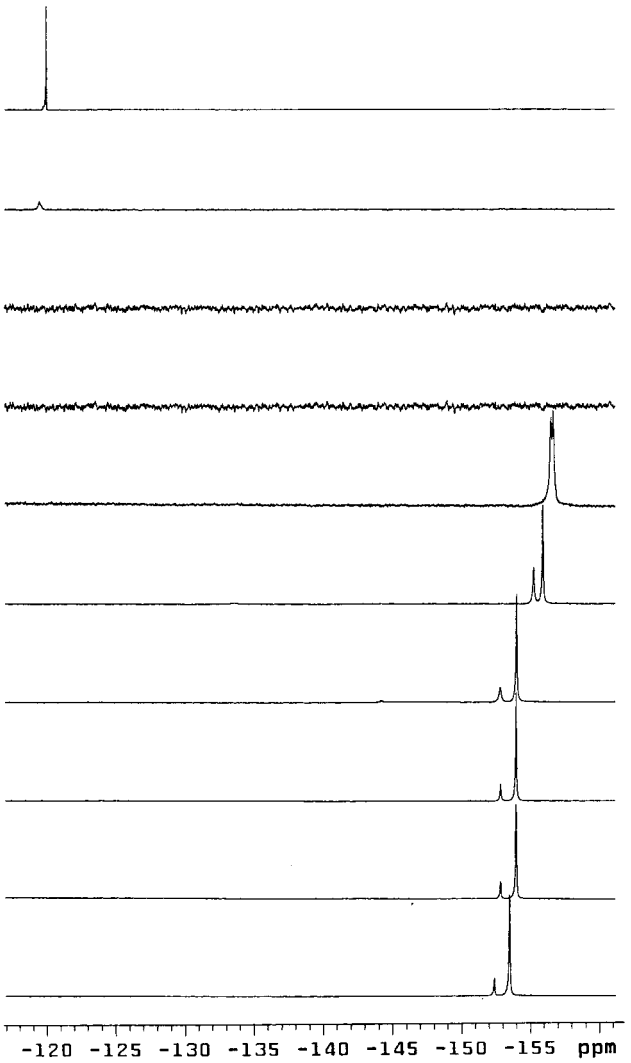

Figure 13. ^{19}F NMR spectra of solution B (2 M $Al(NO_3)$, 2.1 M morpholine, and 1 M HF in water) vs pH (=0.5, 1, 1.5, 2.5, 4, 4.5, 7, 10, 11, and 13.5 from bottom to top).

number of experimental data points are rather few, the derived pK values may be somewhat unreliable. However, the calculated pK_1 value of 3.2 is in acceptable agreement with previous literature reports of pK_1 = 3.7.[20] From these results, the maximum concentration of HF_2^- in solution is obtained at pH $\approx$ 3.2. At this pH, the three F species (HF, F^-, and HF_2^-) contribute approximately equally to the total F concentration in the solution.

Figure 13 shows the ^{19}F NMR spectra of solution B vs pH. For pH $\leq$ 4.5, two well separated peaks, assigned to AlF^{2+} (high field) and AlF_2^+ (low field)[20,21] are observed. If the concentration of other $AlF_x^{(3-x)}$ species ($x \geq 3$) are too small to be observable (due to limited solubility of Al), the ^{19}F NMR signal intensity can be calculated from eqs 4 and 5. The results are indicated in Figure 14 (solid curve) and show qualitative consistency between observed and calculated intensities within the whole pH range investigated. At pH = 13.5, all F is observable as F^-.

The calculated signal intensities (eqs 4 and 5) of the different $AlF_x^{(3-x)}$ ion complexes ($x \geq 1$) are shown by the dashed curves in Figure, 14. When increasing pH from 2.5 to 4.0−4.5, some AlF_3 is expected to be formed (10−30%). From previous reports,[23] the chemical shift of this latter species is expected to appear at a lower magnetic field strength.

Thus, with increasing pH (pH = 4.0 and 4.5), either three separate peaks or some broader resonance band(s) shifted

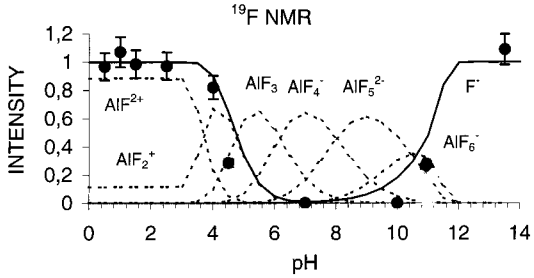

Figure 14. ^{19}F NMR signal intensity vs pH of solutions B ((●) 2 M $Al(NO_3)_3$, 2.1 M morpholine and 1 M HF in water). The solid curve represents calculated signal intensities (eqs 4 and 5) as described in the text. The calculated intensities of the different F species are shown by dotted curves.

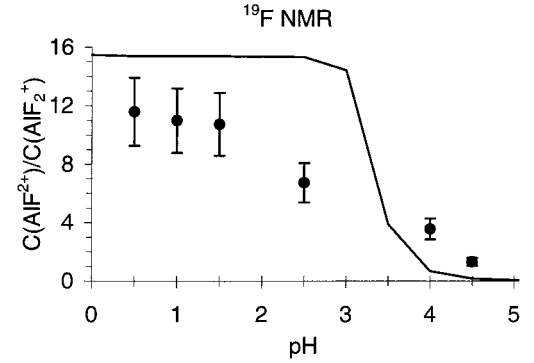

Figure 15. Concentration ratio between the AlF^{2+} and AlF_2^+ species (from Figure 13) in solution B ((●) 2 M $Al(NO_3)_3$, 2.1 M morpholine, and 1 M HF in water). vs pH. The solid curve represents calculated concentration ratio (eqs 4 and 5).

towards a lower magnetic field strength (caused by chemical exchange between the three species) are expected to appear in the spectrum. The coalesce of the AlF^{2+}/AF_2^+ peaks with increasing pH, combined with a reduction in the total observable F signal intensity, supports the assumption that a third, non-observable F species (AlF_3(s)) is formed, which exchanges with the other two F species at an intermediate/fast exchange rate.[23] It should be kept in mind that the experimental uncertainty in pH is approximately ±0.5 units.

As can be inferred from Figure 14, almost all added HF is expected to be found as AlF^{2+} and AlF^{2+} in the pH range from 0.5 up to approximately 4. This is consistent with the ^{27}Al NMR data discussed in the previous section. This multinuclear consistency has, to our knowledge, not previously been reported.

When plotting the observed concentration ratio between AlF^{2+} and AlF^{2+} (Figure 15), only a qualitative agreement between observation and calculation (eqs 4 and 5) is obtained. This may suggest that the reported equilibrium constants used in the model calculation (eq 5) may be slightly erroneous. Another feasible explanation is that the implicit assumption (made in the model calculation) that all dissolved species have activity coefficients of unity is not correct. An activity coefficient of unity indicates diluted aqueous solutions, which is certainly not realized in this work. However, this work suggests that NMR can be used to derive equilibrium constants vs pH of many of the reactions depicted in eqs 4 and 5. However, this interesting aspect is outside the scope of the preliminary investigation presented in this work.

Conclusion

^{27}Al, ^{19}F, ^{13}C, and ^{1}H NMR measurements at room temperature of two aqueous solutions containing $Al(NO_3)_3$ and

morpholine, in the presence and absence of HF, suggest that morpholine is an inert species, the chemical shifts of which (proton and carbon) can be used to estimate the pH of the solution;

The-broad peaks observed in the ^{19}F and ^{27}Al NMR spectra are consistent with the formation of multinuclear Al species and Al−F complexes (AlF^{2+} and AlF_2^+). The observed signal intensities as a function of pH are in qualitative agreement with corresponding intensities calculated from chemical equilibrium reaction models. A more detailed analysis of the NMR spectra reveals discrepancies between observed and calculated intensities, which may tentatively be ascribed to the assumption of (a) unity activity coefficients of all species and/or (b) slightly erroneous equilibrium constants used in the model calculations.

The results suggest that NMR is a well-suited spectroscopic technique for the determination of activity coefficients/equilibrium constants for many of the main chemical reactions involved. This is of importance when aiming at calculating the equilibrium concentrations of actual species in a real SAPO synthesis solution at different synthesis conditions. One disadvantage of the technique is that some of the species are not observable due to severe line broadening originating from different types of molecular exchange processes (intermediate rates) taking place. Some of these limitations may be overcome by studying the synthesis solutions at elevated temperature.

References and Notes

(1) Flanigen, E. M.; Lok, B. M.; Patton, R. L.; Wilson, S. T.; 7th IZC, Tokyo, 1986, 103−112.
(2) Hasha, D.; Sierra de Saldarriaga, L.; Saldarriaga, C.; Hathaway, P. E.; Cox, D. F.; Davis, M. E. *J. Am. Chem. Soc.* **1998**, *110*, 2127−2135.
(3) Wilson, S. T.; Lok, B. M.; Flanigen, E. M.; U.S. Patent 4,310,440, 1982.
(4) Guth, F.; Kessler, H.; Couriers, T. D. U.S. Patent 5,096,684, 1992.
(5) Mortlock, R.F.; Bell, A. T.; Radke, C. J. *J. Phys. Chem.* **1993**, *97*, 767−774.
(6) Akitt, J. W.; Eldres, J. M. *J. Chem. Soc. Dalton Trans.* **1988**, 1347−1355.
(7) Vistad, Ø. B.; Hansen, E. W.; Akporiaye, D.; Lillerud, K. P.; *J. Phys. Chem.*, submitted.
(8) Akitt, J. W.; Farthing, A. *J. Magn. Res.* **1978**, *32*, 345−352.
(9) Akitt, J. W.; Gessner, W.; *J. Chem. Soc. Dalton Trans.* **1984**, 147−148.
(10) Kinrade, S. D.; Swaddle, T. W. *Inorg. Chem.* **1989**, *28*, 1952−1954.
(11) McCormick, A. V.; Bell, A. T.; Radke, C. J.; *J. Phys. Chem*. **1989**, *93*, 1741−1744.
(12) Mortlock, R. F.; Bell, A. T.; Chakraborty, A. K.; Radke, C. J. *J. Phys. Chem.* **1991**, *95*, 4501−4506.
(13) McCormick, A. V.; Bell, A. T.; Radke, C. J. *Zeolites* **1987**, *7*, 183−190.
(14) Ciavatta, L.; Iuliano, M.; Porto, R. *Polyhedron* **1988**, *7*, 1773−1779.
(15) Dean, P. A. W.; Evans, D. F. *J. Chem. Soc. A* **1967**, 698−701.
(16) Dean, P. A. W.; Evans, D. F. *J. Chem. Soc. A* **1970**, 2569−2574.
(17) Busey, R. H.; Schwartz, E.; Mesmer, R. E. *Inorg. Chem.* **1980**, *19*, 758−761.
(18) Marat, R. K.; Janzen, A. F. *Can. J. Chem.* **1977**, *55*, 3845−3849.
(19) Duncan, T. M.; Douglas, D. C.; Csencsits, R.; Walker, K. L. *J. Appl. Phys.* **1986**, *609*, 130−136.
(20) Connick, R. E.; Poulson, R. E. *J. Am. Chem. Soc.* **1957**, *79*, 5153−5157.
(21) Matwiyoff, N. A.; Wageman, W. E. *Inorg. Chem.* **1970**, *9*, 1031−1036.
(22) Buslaev, Y. A.; Petrosyants, S. P. *Koord. Khim.* **1979**, *5*, 163−170.
(23) Sur, S. K.; Bryant, R. G. *Zeolites* **1996**, *16*, 118−124.
(24) Mortlock, R. F.; Bell, A. T.; Radke, C. J. *J. Phys. Chem.* **1993**, *97*, 775−782.
(25) Wilson, M. A.; Collin, P. J. *Anal. Chem.* **1989**, 1253−1259.
(26) Karlik, S. J.; Elgavish, G. A.; Pillai, R. P.; Eichhorn, G. L.; *J. Magn. Reson.* **1982**, *49*, 164−167.
(27) Bradley, S. M.; Kydd, R. A.; Yamdagni, R. *J. Chem. Soc. Dalton Trans.* **1990**, 2653−2656.
(28) Akitt, J. W.; Greenwood, N. N.; Lester, G. D. *J. Chem. Soc. A* **1971**, 2450−2457.
(29) Led, J. J.; Gesmar, H. *Chem. Rev.* **1991**, 1413−1426.
(30) Harris, R. K. *Nuclear Magentic Resonance Spectroscopy − a Physicochemical View*; Pitman Books Limited: London, 1983; p 138.
(31) Lide, D. R., Ed. *Handbook of Chemistry and Physics*, 74th ed.; Chemical Rubber Press Inc.: Boca Raton, 1993/1994; p 8−44.
(32) Stumm, W.; Morgan, J. J. *Aquatic Chemistry - An Introduction Emphasizing Chemical Equilibria in Natural Waters*, 2nd ed.; J. Wiley & Sons: New York, 1981; p 241.
(33) Marcuccilli-Hoffner, F. Etude des milieux de synthese fluores de zeolithes et d'aluminophospates microporeaux. Thèse, Universite de haute Alsace, France, 1992.